A new in situ methodology for the quantification of the oxygen storage potential in perovskite-type materials

(Article begins on next page)

12 May 2024

A new *in situ* methodology for the quantification of the oxygen storage potential in perovskite-type materials

Giuliana Magnacca*[a], Giulia Spezzati[a], Francesca Deganello[b], Maria Luisa Testa[b]

[a] Università di Torino, Dipartimento di Chimica e NIS Centre of Excellence, Via P. Giuria 7, I-10125 Torino, Italia.

[b] Consiglio Nazionale delle Ricerche (CNR), Istituto per lo Studio dei Materiali Nanostrutturati (ISMN), UOS-PA, via U. La Malfa 153, I-90146 Palermo, Italia.

A well known perovskite-type material, $LaFeO_3$, was prepared by citrate-nitrate auto-combustion synthesis and used to formulate a new i*n situ* approach for the analytical evaluation of the redox properties of this class of materials. Carbon monoxide was used as reducing agent-probe, while molecular oxygen was used as oxidizing agent-probe. *In situ* FTIR spectroscopy was applied for a qualitative characterization of the interaction probe-material, and microgravimetry was used in order to quantify the extent of such interaction. The results obtained indicated that simple molecules, such as CO and O_2, are able to define the redox properties of the material without inducing any important modification as in the case of the more classical temperature –programmed reduction and oxidation methods. The described procedure can be successfully applied for the evaluation of the oxygen mobility/availability and storage potential of other perovskite-type materials.

Introduction

The effectiveness of perovskite-type materials in applications concerning, among others, catalysis [1, 2, 3], photocatalysis [4,5] and fuel cells [6,7] is well known. It is demonstrated, for instance, that oxygen atoms present in the lattice of a perovskite-type material can be removed or restored very easily [8, 9]. This has been found to depend mainly on the presence of structure defects [8,10], which is subordinated to the type of perovskite structure system, although it can be optimized by a careful choice of dopants [10-12]. The oxygen availability depends as well on the conditions of materials synthesis and processing [13-15]. This feature may be used to control the oxidation reactions, where lattice oxygen can be replaced by the less convenient and too active gas phase molecular oxygen, for the oxidation of substrates [16] such as, for example, CO and hydrocarbons [17]. Moreover, the high oxygen conductive properties of perovskite make this material highly attractive for energetic purposes, i.e. as constituent of solid oxide fuel cells (SOFCs) [7,11,18-21], as well as for membranes for oxygen separation [22] and for gas sensor [23] or biosensor [14] applications.

In particular, $LaFeO_3$ is a very well known perovskite-type compound. As it is or doped with alkaline ions, it can be easily and conveniently used as photocatalyst [24], since it absorbs the light in the VIS range with a proved photoactivity in dyes decomposition, resulting even better than TiO_2 Degussa P25 oxide [4].

Although the use of perovskites as catalysts, photocatalysts and electrocatalysts is widely accepted, only few trials were made to identify and quantify the active species responsible for their activity [10,25]. In most cases, the assessment of material goodness is simply made using the material in an applicative process [11,26], or following the degradation of the materials via Temperature Programmed Reduction (TPR), Oxidation (TPO), Desorption (TPD) and O_2-pulse measurements [12,27-29]. The temperature programmed methods are widely used to study the availability of labile oxygen or the reactive oxygen at high temperature, but they fail in the

determination of the *in situ* reactive oxygen. Other methods used to investigate qualitatively or quantitatively the oxygen availability of perovskite-type materials include X-ray Photoelectron Spectroscopy [29-30], Secondary Ion Mass Spectrometry, Isothermal Isotope Exchange [31] and Oxygen Isotopic Exchange [28] for the surface oxygen, and Thermogravimetric Analyses [10-11, 32], Diffuse Reflectance FTIR Spectroscopy [33], Near Edge X-ray Absorption Fine Structure [11] and Oxygen Isotopic Exchange [28] for the bulk oxygen. Nevertheless, most of these procedures allow to perform only phenomenological determinations and cause loss/deterioration of materials and consume of reagents. The aim of this paper is to individuate a simple, inexpensive and not-aggressive *in situ* methodology for determining the redox properties of a perovskite-like system. In order to obtain a quantitative determination of the oxygen availability and/or oxygen loading, the redox process was monitored *in situ* under a controlled atmosphere. Carbon monoxide was used to create a reducing atmosphere, while molecular oxygen was used to create an oxidant environment.

Basic concepts on the quantification of oxygen availability and oxygen loading

Oxygen availability and oxygen loading are strictly related to the oxygen-storage potential of perovskites. In fact, the oxygen-storage process could be divided in two steps. In the first step, indicated as "oxidizing step", the oxygen species leaves the perovskite structure in order to oxidize substrates and it is possible to study the oxygen availability. The oxygen loading, related to the oxygen enrichment of perovskite structure, can be studied in the second step called "oxygenating step".

Oxygen availability can be determined considering the high affinity between $LaFeO_3$ and carbon monoxide [23]. In the absence of adsorbed molecular oxygen, CO can form carbonate-like groups only if mobile and available oxygen species are present on material surface, due to a redox reaction between CO and lattice oxygen atoms. The reaction can be followed via FTIR spectroscopy in which carbonate-like species show typical IR signals in the range 1800-1100 cm^{-1} and the extent of the reaction can be evaluated quantitatively considering the increase of sample mass via microgravimetric determinations after CO contact. Only the fraction of mobile oxygen closest to the surface of the perovskite was determined, since only oxygen present in the outermost layer of the material can diffuse into the material and reach CO on the surface for the carbonate formation.

On the other hand, the amount of available oxygen atoms is related to the oxidation state of iron, almost no redox effects due to lanthanum are recognized by scientific community [34]. The redox properties of the species $Fe^{\circ}/Fe^{2+}/Fe^{3+}$ are considered by several authors the driven force necessary to this material to explicit its oxygen storage function.

In these terms, the oxidation state of iron can be related to the presence of mobile oxygen, and, once more, carbon monoxide can be used as a probe for determining the iron oxidation state. Finally, oxygen loading can be measured directly in the microgravimetric apparatus following the mass change of material in the presence of molecular oxygen. Oxygen can interact in two different ways, via molecular adsorption and via dissociative adsorption. The first contribute is not interesting for our purposes, because oxygen molecules are very weakly bonded to the perovskite surface and need a subsequent activation to form ions and penetrate the material structure in the "oxygenation phase". The second contribute enriches directly the perovskite structure of oxygen species. This amount is strictly related to the perovskite oxidizing power which is actualized in the "oxidative phase". While the first contribution leads to a reversible adsorption, the second one produces an irreversible interaction. Thus, it is necessary to carry out an adsorption and a following desorption to obtain the effectively active oxygen loading.

The advantage in using carbon monoxide is twofold. On one hand, it can be used as a probe molecule to test the oxidation state of the material surface and its spectroscopic stretching frequency can give qualitative information on the species formed on the material surface after a redox treatment. On the other hand, it possesses redox properties, since it could reduce the material in presence of active oxygen by forming CO_2. Subsequently, the interaction between CO_2 and surface oxygen atoms causes the formation of carbonate-like species, whose spectroscopic features allow to identify the species formed, whereas microgravimetric determinations allow to quantify the interactions.

Experimental

Materials

Ultrapure CO and O_2 compressed gases were supplied by Praxair.

$LaFeO_3$ was prepared by citrate-nitrate auto-combustion synthesis (CNA) by improving the method already described in the literature for other perovskite-type compounds [35]. $La(NO_3)_3$ $\cdot 9H_2O$ (99.9%, Aldrich), $Fe(NO_3)_3$ $\cdot 9H_2O (\geq 98\%$, Carlo Erba) were carefully weighted in the required proportions, poured in a 1.2 L stainless steel beaker and dissolved in distilled water at RT under magnetic stirring. Ammonium nitrate (BioXtra, $\geq$99.5%, Sigma Aldrich) and citric acid (99.9 %, anhydrous, Fluka), were then added to the metal precursor solution as oxidant additive and propellant-template-complexant, respectively. Ammonia solution (30 vol%NH_4OH, Aldrich) was finally added as a pH regulator and the pH was set to 6. The citric acid/metal salts molar ratio was set to 2, while the reducers/oxidizers ratio was set to the stoichiometric value for the specific combustion reaction, following the method described by Jain *et al*. [36]. The water was left to evaporate at 80°C (a vertex was inserted in the precursor solution) under constant magnetic stirring until the formation of a homogeneous gel. Initiation of the combustion reaction was performed by putting the stainless steel beaker on a hotplate and setting the temperature at around 200°C. The as-burnt powder was calcined at 700°C for 5h for the complete crystallization of the perovskite-type phase.

Methods

Structural and morphological characterization

Specific surface area and porosity were determined by studying the gas-volumetric N_2 uptake at 77K using an ASAP2020 by Micromeritics. BET model [37] was applied for specific surface area determination and BJH model [38] was used for porosity characterization. Sample analyses were performed after outgassing *in vacuo* (residual pressure $\sim 10^{-2}$ mbar) for several hours at 200°C in order to reach a good surface cleaning.

X-ray diffraction (XRD) measurements were carried out on a SIEMENS D5000 X-ray powder diffractometer equipped with a Kristalloflex 760 X-ray generator and with a curved graphite monochromator that made possible the selection of the Cu Kα radiation (40 kV/30 mA). The 2θ step size was 0.03°, the integration time was 3 s per step, and the 2θ scan range was 18 - 88°. The diffraction patterns were analyzed by Rietveld refinement using the GSAS package [39]. Chebyschev polynomials and Pearson VII functions were chosen for the background and for the peak profile fitting, respectively. In the structure refinement lattice constants, zero offset, scale factors, FWHM, Debye Waller factors and microstrain were considered as variable parameters. From fitting results, the structural parameters of the investigated compounds and, in particular, the cell edge lengths were obtained. Moreover, an estimation of the crystal size values was obtained from Scherrer equation, in agreement with the GSAS package procedure [39]. A graphical analysis of the fit, the chemical reasonableness of the model and the acceptability of

the discrepancy values (goodness of fit "χ^2" and reliability factors "R factors") were all used for judging the quality of the Rietveld refinement [40]. The most straightforward R factor is the weighted profile R factor (R_{wp}), which is the square root of the quantity minimized, scaled by the weighted intensities; the goodness-of-fit, χ^2, is defined as $(R_{wp}/R_{exp})^2$, where R_{exp} is the best possible R_{wp}; the reflection-based factor, R_F^2 (also called R_{Bragg} factor), is the agreement between the observed and computed reflection. Discrepancy values are only statistically defined parameters and they are generally acceptable when χ^2 is close to 1 and R factors are lower than 10%, although high instrumental resolution and larger number of counts might often increase the R factors, without necessarily resulting in a lower quality of the model. A standard deviation of ±0.003 Å for the refined cell parameters was estimated for the experimental conditions used in this work.

High-Resolution Transmission Electron Microscopy was performed on a JEOL JEM 3010UHR (300 kV) TEM fitted with a single crystal LaB6 filament. Sample was dry deposited on Cu "holey" carbon grids (200 mesh).

Sample pretreatment

Redox properties of materials were obtained by means of adsorption measurements using CO and O_2 as adsorptive molecules. Pretreatment of the samples before the adsorption process was made as follows. To obtain the room temperature sample, the pellet was simply treated *in vacuo* for 60 minutes to obtain the reference sample. To obtain reduced samples, the pellets were activated *in vacuo* for 60 minutes at the desired temperature, being well known the reducing power of thermal treatment *in vacuo* at high temperatures. To obtain oxidized samples, the pellets were treated 20 minutes *in vacuo* at the desired temperature, 20 minutes in 100 mbar of O_2 and again 20 minutes *in vacuo* at the same temperature. After that, the samples were cooled down at RT *in vacuo*. The extension of the oxidizing time and/or of the final outgassing during the cooling down of the material does not modify the oxidation state of the sample. Samples are indicated in the text as $LaFeO_3$ XT, where X can be R (Reduced, after *in vacuo* activation) or O (Oxidized, after O_2 pretreatment), and T indicates the temperature of the pretreatment in Celsius degrees (400 or 700°C). Therefore, $LaFeO_3$ R400 indicates a sample outgassed *in vacuo* at 400°C whereas $LaFeO_3$ O400 indicates a sample oxidized at 400°C.

FTIR characterization

FTIR spectra in the range 4000-700 cm^{-1} were obtained by means of Bruker 113v spectrophotometer equipped with Globar source and MCT cryodetector at the resolution of 4 cm^{-1}. Samples, in form of self supporting pellet of about 40 mg cm^{-1}, were placed in a home-made quartz cell equipped with KBr windows for pretreatment and analyses.

The adsorption of CO on prepared samples was made by contacting the samples with 100 mbar of CO. After that, the oxidized samples were kept in contact with CO for up to 16 hours, in order to check the reducibility of the surface in the presence of CO. Otherwise, the reduced samples were out-gassed step-by-step for up to 10 minutes to remove the reversibly bonded CO adsorbed species. During the spectroscopic experiments, spectra were recorded time by time to check any *in situ* modification.

Microgravimetric characterization

Adsorption microgravimetric experiments of reduced and oxidized powders were performed in a microbalance apparatus IGA002 by Hiden with quartz sample holder, quartz reactor and fast response furnace able in heating samples in the range RT-1000°C. Before adsorption measurements, $LaFeO_3$ sample was activated *in vacuo* at 25°C, then oxidized and reduced at 400 and 700°C and, for each treatment, the interaction with CO gas was evaluated.

In order to measure the oxygen availability, a known amount of carbon monoxide (100 mbar) was admitted in the sample chamber and left there for a prolonged time (primary interaction). After that, sample was outgassed *in vacuo* until mass stabilization was reached and finally submitted to a new, prolonged contact with CO (secondary interaction).

Microgravimetric measurements of oxygen loading were carried out evaluating the mass change of material after prolonged contact with oxygen molecules in the gas phase at 400°C and 700°C, and after a subsequent outgassing at 25°C until mass stabilization was reached.

The samples weight was continuously controlled during the microgravimetric measurements.

Results and discussions

Structural and morphological characterization of the LaFeO3 powder

In Figure 1 the Rietveld refinement of the $LaFeO_3$ powder after calcinations at 700°C for 5h is reported, together with the discrepancy values. The crystalline material formed is single-phase and it shows the structure of orthorhombic perovskite-type $LaFeO_3$ (space group Pbma) with cell parameters of 5.573 Å, 7.859 Å, 5.560 Å in agreement with the ICSD database (n°164083). It possesses a crystal size of 80 nm, a microstrain of 0.326 %, a specific surface area (BET model) of 15.1 $m^2 g^{-1}$ and a mesoporosity (BJH model) of 0.13 cm^3/g obtained from desorption data. BJH curves relative to pore size distribution curve are reported in Figure 2. A bimodal distribution of pores which are centered at about 20 and 270 Å of width is visible.

Figure 3 reports the TEM images of $LaFeO_3$ obtained at three magnifications. Section A allows to evidence particles morphology and size. Particles possess roundish irregular shape evidencing coalescence of spherical moieties (more evident in section B) probably due to the high temperature thermal treatment. Primary particles show diameters in the range 50-150 nm, with an average size of about 80-100 nm, in good agreement with Rietveld analysis indications. In section B it is possible to observe the presence of small pores (less than 5 nm of width), present both at the interface between fused particles and inside the particles. Finally, section C reports the image of a particle with evident interference fringes pattern (d_{hkl} = 3.89 Å) assigned to the plane (100) of $LaFeO_3$.

FTIR spectroscopy: outgassing pattern

Figure 4 shows the typical spectra of $LaFeO_3$ in medium-IR range, obtained by outgassing the perovskite *in vacuo* at increasing temperatures. In the range 3700-3000 cm^{-1}, ν_{OH} signals are visible relative to free (~3700 cm^{-1}) and H-bonding (the wide and intense signal at 3650-3000 cm^{-1}) OH groups on the surface. After a thermal treatment at 300°C the intense H-bonding interacting groups signal is not visible anymore. Moreover, due to a thermal treatment at 600°C also the free OH groups signal disappears, indicating the complete removal of the hydrated layer. ν_{CH} signals at ~3000 cm^{-1} can be ascribed to the hydro-carbonaceous residues probably originated by a partial decomposition of citrate molecules during the synthesis of material. They reduce their intensity only after treatment at 400°C.

At ~2345 cm^{-1} a weak signal given by Σ_u^+ vibrational signal of CO_2 molecules is visible and disappears only after a vacuum treatment at high temperature (∼600°C).

A signal at 1630 cm^{-1} due to δ_{HOH} of water molecules is visible only for the air-exposed sample.

An intense band pair at ~1600-1500 cm^{-1} is attributed to carbonate-like groups formed during the synthesis of material. In fact, the fraction of organic species completely oxidized in combustion process forms CO_2 which, together with atmospheric CO_2, strongly binds to the basic oxygen of perovskite. This bond is gradually broken by an increase of the activation temperature.

A very weak pair of signals is observable at ~1000 cm^{-1} and their relative intensity changes with the pretreatment temperature. It is possible to observe the stronger signal at higher wavenumbers for hydrated samples, treated at low temperature, while the prevalent signal is at lower wavenumbers for dehydrated samples treated at high temperature. This seems to indicate that the couple of bands is sensitive to the presence of adsorbed species. Since they are very weak and their frequency is almost double in respect to one of the principal band of material (at 560 cm^{-1} is present the bending of O-Fe-O [41]), we can assign the bands to the harmonic mode of outermost O-Fe-O groups bending signal, changing their intensity with surface environment. Finally, the intense signals visible at ~700 cm^{-1} are probably due to bulk vibrations of LaFeO$_3$. Only small variations are evidenced in the spectra following the same thermal activation procedure in oxidizing conditions, thus the oxidized sample pattern will not be shown.

The FTIR spectra are essentially similar to those described by Li et al [41], although some small absorptions were not detectable in Li's spectra because of the sample dilution in KBr used in those experiments.

The trend shown by ν_{OH} signals indicates that the increase of the temperature in the thermal treatment carries out the progressive elimination of OH groups interacting via H-bonding with water molecules or with other OH groups present at the surface.

The ν_{CH} signals, not easily removed from the material and still visible after a thermal treatment *in vacuo* at 400°C, indicate that hydrocarbonaceous residues interact strongly with perovskite material.

For what concerns the Σ_u^+ vibrational signal of CO$_2$ at ~2345 cm^{-1}, is still visible after the *in vacuo* treatment. This suggests that CO$_2$ molecules, as well as the hydrocarbonaceous residues described above, could be entrapped in the closed porosity of the material. Only when the structure is modified after a treatment *in vacuo* at high temperature (~600°C), the pores open and the 2345 cm^{-1} signal disappears from the spectrum because entrapped contaminants are removed from the sample. This is a very important aspect to be considered when dealing with photocatalytic tests of perovskite-type materials in water solution, because there might be enhancement/suppression of the catalytic activity of the material under study, when the entrapped organics leaves the closed porosity and dissolves in water solution. Therefore, a sonication treatment in a water suspension was carried out on LaFeO$_3$ with the aim of checking the material stability. The results of specific surface area and porosity measurements, obtained after sonication, indicate that the material was slightly modified with an increase of the specific surface area from the initial 15.1 m^{2}g^{-1} to 18.1 m^{2}g^{-1} as well as of the total porosity from 0.13 cm^{3}g^{-1} to 0.23 cm^{3}g^{-1} and a modification of the average pore width (visible in the comparison reported in Figure 2). This confirms that both the sonication treatment and the thermal treatment *in vacuo* are able to modify the sample, making visible part of the surface relative to the closed porosity of the as-synthesized material. This aspect will be examined in detail in a forthcoming paper.

The water band (~1630 cm-1) removed after a simple treatment at RT indicates that the material does not have great affinity with water. In fact, water band removal after a mild treatment should indicate that water molecules do not interact very strongly with material surface. This is be an evidence of a scarce surface hydrophilicity, which conversely means a quite good hydrophobicity. Considering the possible applications of this material in (photo)catalysis, this feature suggests that only hydrophobic substrates can actively interact with this material in order to undergo a (photo)degradation in a photocatalytic reaction, where the first step involves the approach of substrates to photocatalysts surface,

The spectral pattern allows to evidence three steps as representative for the study of sample behaviours: the activation at RT to obtain samples completely hydrated and not modified by any thermal treatment, the activation (reducing and oxidizing conditions) at 400°C to obtain samples submitted to an almost complete dehydration and to a medium degree of surface cleaning (*i.e.*, removal of surface functional groups), and, finally, the activation (reducing and oxidizing conditions) at 700°C to obtain samples surface almost completely cleaned up and highly reactive towards probe molecules. Therefore, in the following paragraphs, the investigation concerning CO interacting with sample simply activated at RT, reduced and oxidized at 400°C, and reduced and oxidated at 700°C, is discussed.

FTIR spectroscopic and microgravimetric results

Figure 5 reports the spectra obtained after CO admission on oxidized (upper section) and reduced (lower section) samples at 400°C. Figure 6 is referred to the same samples (oxidized, section A, and reduced, section B) in the lower wavenumber region (1900-800 cm^{-1}). The ν_{CO} signals at wavenumber < 2140 cm^{-1} indicate the presence of π-backdonation, possible only if d-electrons are present on iron orbitals, *i.e.*, in the presence of Fe^{n+} cations with n < 3. The signal at 1980 cm^{-1} is assignable to CO-Fe° [42], and the signals at wavenumbers lower than 1980 cm^{-1} are probably due to bridged carbonylic species.

When the spectra of $LaFeO_3$ O400 in the 2300-1800 cm^{-1} region (Figure 5, upper section) is examined, a very limited intensity bands at wavenumber < 2140 cm^{-1} are present, indicating few surface species Fe^{n+} with n<3. Waiting up to 16 hours, some components increase in intensity and specific signals at ~2040 and 1900 cm^{-1}, together with the less important bands in the range 2000-1900 cm^{-1}. That indicates that CO prolonged contact is modifying $LaFeO_3$ surface decreasing the Fe^{n+} oxidation state, even at RT.

The spectra of the same sample in the 1900-800 cm^{-1} range (Figure 6A) show again limited spectral modifications induced by CO presence, at least during the first contact with the gas. When the contact is prolonged during 16 hours the formation of new wide bands at ~1500, 1350 and below 1200 cm^{-1} are evident (see differential spectra). These bands allow to identify monodentate and bidentate carbonates of through the couples of bands splitted of about 150-180 cm^{-1} [43]. This fact suggests that oxygen atoms, interacting with CO oxidation products, are not of the same type [44].

The starting spectrum of CO gas contacted with $LaFeO_3$ R400 in the 2300-1700 cm^{-1} region (Figure 5, lower section) shows a more complex shape, due to the presence of signals at 2080, 2050 and a doublet at around 2000 cm^{-1}. At lower wavenumber, a couple of large signals is visible in the 1950-1800 cm^{-1} range. After the CO outgassing, the described bands shift to lower frequencies and, moreover, it is possible to observe a weak signal at ~2080 cm^{-1} , some intense bands at ~2040 and 2000 cm^{-1} and a couple of bands at ~1900 and 1830 cm^{-1} whose intensity increased. All ν_{CO} signals at wavenumbers < 2140 cm^{-1}, indicate the presence of Fe^{n+} with n<3.

At lower wavenumbers (Figure 6B) the modifications induced by CO presence are much more limited, as indicated by the very low intensity of differential spectra.

Figure 7 reports the spectra obtained after CO admission on the oxidized (upper section) and reduced (lower section) sample at 700°C, while Figure 8 reports the spectra of the same samples oxidized (section A) and reduced (section B) in the lower wavenumber region.

The spectra of CO interacting with $LaFeO_3$ O700 (Figure 7, upper section) show the presence of a weak signal at ~2170 cm^{-1} and some intense bands at wavenumber <2140 cm^{-1}, in particular a broad envelope is present in the range 2140-2000 cm^{-1}. Also a couple of wide bands at ~1900 and 1830 cm^{-1} is present. During outgassing, CO signals change intensity and shift to lower

wavenumbers; after 16 hours of CO contact an intense signal at ~2040 and two complex absorptions at around 2000 and in 1900-1800 cm^{-1} range appear and become predominant in the spectra.

In the low frequency range (Figure 8A) some complex bands appear at about 1500 and 1300 cm^{-1} during the contact with CO and shift at ~1580 and 1340 cm^{-1} after 16 hours of contact with CO.

The analysis of LaFeO$_3$ R700 spectra shows a very different situation. In the high frequency range (Figure 7, lower section) it is not possible to observe any signal at wavenumbers > 2140 cm^{-1}. At the beginning of the experiment an envelope of at least four components is present in the range 2100-1950 cm^{-1} as well as the couple of bands at ~1900 and 1830 cm^{-1}. CO pumping off does not cause any important modification of the spectra, except for the signal at ~2100 cm^{-1} which disappears.

Similarly, in the carbonate-like absorption region (Figure 8B) the modification of the spectra is almost irrelevant.

The microgravimetric data are reported in Table I. They are expressed in percentage of mass, respect to the mass of the sample before CO contact, in order to obtain a direct comparison among all the results.

The amounts of oxygen captured by the samples, and reported in percentage of mass with respect to the mass of the sample before oxygen interaction, are the following: 0.010 for LaFeO$_3$ O400 and 0.121 for LaFeO$_3$ O700.

Table I. Microgravimetric results: amounts of CO (expressed in % mass) interacting with LaFeO$_3$ activated in different conditions.

Sample	Primary interaction (% mass)	Secondary interaction (% mass)	Total interaction (% mass)
LaFeO$_3$ RT	0.010	0.003	0.013
LaFeO$_3$ O400	0.216	0.035	0.251
LaFeO$_3$ O700	0.374	0.019	0.393
LaFeO$_3$ R400	0.147	0.004	0.151
LaFeO$_3$ R700	0.311	Not measurable	0.311

The most relevant results can be summarized in the following.

1) CO interaction with RT-activated sample

When CO comes in contact with the RT-activated sample, no adsorbed species are formed since no FTIR signals form in MIR spectral region, neither CO adsorption can be evidenced by microgravimetric results. This indicates that this sample: a) does not possess coordinatively unsaturated Lewis acid sites, probably because the activation temperature is not enough high to clean the surface from adsorbed water and/or carbon dioxide deriving from atmosphere-material interactions, or b) does not possess oxygen ions available for the formation of carbonates, probably because they are not activated by the thermal treatment carried out at RT.

2) CO interaction with 400°C-activated sample

The oxidation at 400°C seems to have modified the availability of oxygen with respect to the activation at RT. The starting spectrum evidences the presence of a limited amount of iron ions which are characterized by low oxidation number. On the other hand, the bands at lowest

wavenumbers increased after 16 hours of contact, indicating that CO itself, for simple contact at RT, is able to reduce the sample without any kind of thermal activation.

In $LaFeO_3$ O400 the presence of oxidized iron ions is responsible for the signals at frequencies higher than 2140 cm^{-1}. These signals tend to disappear increasing the contact time CO/sample, indicating the reductive effect carried out by CO at RT.

$LaFeO_3$ R400 does not show any signal at frequencies higher than 2140 cm^{-1}, indicating the complete absence of coordinatively unsaturated Fe^{3+} ions. Otherwise, several signals are present at low wavenumbers, indicating the interaction of CO with reduced iron ions. Also in this case, the contact of the sample with CO overtime shifts all the signals to lower wavenumbers, indicating the progressive reduction of the sample operated by CO.

In the 1800-1100 cm^{-1} range (figure 6B), carbonate groups show their typical signals, indicating an increase of oxygen available to CO reaction. The relative intensity of the bands indicates that the formation of carbonate groups is limited for reduced $LaFeO_3$, and that this sample possesses a limited amount of available oxygen. This feature is also confirmed by microgravimetric quantitative data.

All the spectra show that CO continues to interact with sample, in particular with oxidized $LaFeO_3$, indicating that the availability of oxygen species varies in time and that a diffusive process relative to oxygen species, which move from internal layers to the surface, occurs. This is witnessed by microgravimetric results, since an activity development is evidenced for oxidized sample during the second CO adsorption run.

Microgravimetric data evidence that the increase of the activation temperature makes samples more active towards CO interaction, especially when an oxidizing treatment was carried out. Reduced samples develop almost all their oxygen storage activity during the primary interaction phase, and no further activity is evidenced in the secondary interaction phase. Otherwise, oxidized samples continue to perform their not negligible activity during the secondary interaction phase, indicating that reactive oxygen species continue to be formed.

The stability of the materials is demonstrated by the outgassing of the sample, reduced or oxidized, at 300°C *in vacuo* which restores the material in the initial form: after this treatment it is possible to repeat the entire sequence of experiments without a significant modification of the spectra.

3) CO interaction with 700°C-activated sample

The material activation at 700°C produces differences between oxidized and reduced samples much more evident than between the samples treated at 400°C. This activation is actually effective in obtaining an oxygen-rich (*i.e.,* reactive towards CO) sample in the case of $LaFeO_3$ O700 and an oxygen-poor (*i.e.,* inert towards CO) sample in the case of $LaFeO_3$ R700.

The oxidation process carried out at 700°C is effective in producing an almost oxidized sample, since signal relative to Fe^{3+} sites are observable in the spectra at ~2170 cm^{-1} in CO spectra. Moreover, sample oxidized at 700°C presents the highest activity due to the best availability of oxygen species, being able in interacting with carbon monoxide to form reduced Fe^{n+} species and intense signals relative to carbonate-like groups. This is in agreement with computational works in which the oxygen species interact preferentially with Fe^{n+} rather than with lanthanum ions, due to the more efficient overlap between hybrid *sp* orbital of oxygen and *3d* orbitals of iron [25, 45]. This implies that oxygen coverage indirectly defines the amount of Fe^{n+} sites through the amount of oxygen vacancies present in the material.

The reduction process carried out at 700°C, on the contrary, produces an oxygen-poor sample which shows iron in reduced form (CO does not form any signal at wavenumber >2140 cm^{-1}), and does not present any ability in oxidizing CO to form carbonate species.

Again, as in the previous case, an outgassing of the sample at 300°C *in vacuo* restores the material in the initial form, and it is possible to repeat the entire sequence of experiments without a meaningful modification of the spectra. The irreversible modification of the sample can be evidenced at a temperature as high as 700°C since the powder becomes dark-green and this happens after several cycles of activation/oxidation.

As in this case of activation at 400°C, prolonged contact with CO causes a continuous variation of the spectra. This is explainable considering a diffusive process relative to perovskite structure oxygen species which move from the bulk to the surface of the material, becoming available for CO reaction. It is worth to notice that this *in situ* process in the presence of CO could be conveniently used for a determination of the oxygen diffusivity in perovskite-type materials for SOFC applications.

The increase of the activation temperature produces very active samples towards CO interaction, in particular when an oxidizing treatment is carried out. The material activated in oxidizing conditions at 700°C, which possesses the largest amount of oxygen active sites, results the most active one.

The activation treatment carried out *in vacuo* at high temperatures induces the perovskite reduction with the formation of a non-stoichiometric compound. This effect becomes more important the higher is the temperature of the thermal treatment. This implies that the activation treatment at 700°C, removes more oxygen from the $LaFeO_3$ than the activation treatment at 400°C. Consequently, during the microgravimetric test, $LaFeO_3$ O700 captures an amount of oxygen about twice higher than $LaFeO_3$ O400.

Also in this case, microgravimetric results indicate that reduced samples develop all their oxygen storage activity during the primary interaction phase (no further activity is evidenced in the secondary interaction phase) and oxidized samples perform their activity during both primary and secondary interaction phases, indicating that the formation of reactive oxygen species is not yet completed.

Conclusions

A new methodology for the *in situ* evaluation of the redox behaviour of perovskite-type materials was developed. The reactivity of simple molecules like CO and O_2 toward a $LaFeO_3$ perovskite-type compound, prepared by a citrate-nitrate auto-combustion route, was followed by FTIR spectroscopy and microgravimetric analyses.

The obtained results indicate that redox properties of the $LaFeO_3$ perovskite are developed at medium-high temperatures, between 400 and 700°C, temperatures at which this material shows enhanced oxygen-storage features. The qualitative predictions obtained by FTIR spectroscopy were confirmed in quantitative terms by microgravimetric results, making this combined FTIR spectroscopy/microgravimetric experiment a real monitoring of oxygen loading on perovskite-type material.

FTIR spectra carried out for several reduction/oxidation cycles suggest that the use of CO/O_2 molecules is not too aggressive for the material, since the sample does not show meaningful modifications after its repeated use.

The advantage in the use of carbon monoxide is multiple. It can be used as a reductive agent, as an oxidation state probe of reducible species and it can be also applied for testing the availability of active oxygen species of perovskite.

This makes the procedure quite interesting for the evaluation of oxygen mobility/availability and storage potential of a perovskite. Moreover, it can be successfully used in combination with other methodologies to have a wide view on the redox properties of perovskite-type materials.

Acknowledgements

References

[a] *Università di Torino, Dipartimento di Chimica e NIS Centre of Excellence, Via P. Giuria 7, I-10125 Torino, Italia. Fax: +39011 6707855; Tel:+39 0116707543; e-mail: giuliana.magnacca@unito.it*
[b] *Consiglio Nazionale delle Ricerche (CNR), Istituto per lo Studio dei Materiali Nanostrutturati (ISMN), UOS-PA, via U. La Malfa 153, I-90146 Palermo, Italia.*

1   J.-A. Villoria, N. Mota, S. A. Al-Sayari, M.-C. Alvarez-Galvan, R.-M. Navarro and J. L. Garcia Fierro, *Micro and Nanosystems*, 2012, **4**, 231-252.

2   N. Labhsetwar, P. Doggali, S. Rayalu, R. Yadav, T. Mistuhashi and H. Haneda, *Chinese Journal of catalysis*, 2012, **33**, 1611-1621.

3   J. Zhu and A. Thomas, *Applied Catalysis B: Environmental,* 2009, **92**, 225-233.

4   Jun Yang, Huiqiong Zhong, Ming Li, Lizhen Zhang and Yuanming Zhang, *React Kinet Catal Lett,* 2009, **97**, 269–274.

5   Z.-X. Wei, Y. Wang, J.-P. Liu, C.-M. Xiao, W.-W. Zeng and S.-B. Ye, *J. Mater. Sci.,* 2013, **48**, 1117-1126.

6   Arumugam Manthiram, Jung-Hyun Kim, Young Nam Kim and Ki-Tae Lee, *J. Electroceram,* 2011, **27**, 93–107.

7   J. Richter, P. Hotappels, T. Graule, T. Nakamura and L. J. Gauckler, *Monatsh. Chem.,* 2009, **140**, 985-999.

8   S. Stolen, E. Bakken, C.E. Mohn, *Phys. Chem. Chem. Phys.*, 2006, **8**, 429-447.

9   A. Weidenkaff, *Adv. Engineering Mater.*, 2004, **6**, 709-714.

10   Zhao Xin, Yang Qiuhua and Cui Jinjin, *J. of Rare Earths*, 2008, **26(4)**, 511.

11   N. Lakshmiranayanan, J.N. Kuhn, S. A. Rykov, J.-M. M. Millet, U.S.Ozkan, *Catal. Today*, 2010, **157**, 446-450.

12   A. Mai, F. Tietz, D. Stover, *Solid State Ionics*, 2004, **173**, 35-40.

13   O. Mihai, D. Chen and A. Holmen, *J. Catal.,* 2012, **293**, 175-185.

14   S. Thirumalairajan, K. Girija, V. Ganesh, D. Mangalaraji. C. Viswanathan, N. Ponpandian, *Cryst. Growth Des.,* 2012, **13**, 291-302

15   C. Nityanand, W. B. Nalin, B. S. Rajkumar, C. M. Chandra, *Solid State Sci.,* 2011, **13**, 1022-1030

16   A. Evdou, V. Zaspalis and L. Nalbandian, *Fuel,* 2010, **89**, 1265; J.E. Readman, A. Olafsen, Y. Larring, and R.Blom, *J. Mater. Chem.,* 2005, **5**, 1931; A.Slagtern and U.Olsbye, *Appl. Catal. A,* 1994, **110**, 99.

17   Kwang-Sup Song, Hao Xing Cui, Sang Don Kim and Sung-Kyu Kang, *Catal. Today,* 1999, **47**, 160.

18   F. Deganello, V. Esposito, M. Miyayama and E. Traversa, *J. Electrochem. Soc.*, 2007, **154**, A89-A96.

19   A. Longo, F. Giannici, A. Balerna, C. Ingrao, F. Deganello and A. Martorana, *Chem. Mater.,* 2006, **18**, 5782–5788;

20   F. Deganello, L. F. Liotta, G. Marcì, E. Fabbri and E. Traversa, *Materials for Renewable and Sustainable Energy*, 2013, **2**, 8.

21   W. Suksamai and I. S. Metcalfe, *Solid State Ionics*, 2007, **178**, 627–634.

22   P.-M. Geffroy, J. Fouletier, N. Richet, T. Chartier, *Chem. Eng. Sci.*, 2013, **87**, 408-433.

23   N. N. Toana, S. Saukko and V. Lantto, *Physica B* 2003, **327**, 279–282.

24   R. Hu, C. Li, X. Wang, Y. Sun, H. Jia, H. Su, Y. Zhang, *Catal. Commun.*, 2012, **29**, 35-39]

25   X. Liu, J. Hu, B. Cheng, H. Qin, M. Zhao and C. Yang, *Sensor Actuat. B-Chem.*, 2009, **139**, 520-526.

26   X.P. Dai, R. J. Li, C. C. Yu, Z. P. Hao, J. Phys. Chem.B, 2006, **110,** 22525-22531.

27   S. Ramesh, M. S. Hegde, *J. Phys. Chem.*, 1996, **100**, 8443-8447.

28   W. Yang, R. Zhang, B. Chen, N. Bion, D. Duprez, S. Royer, *J. Catal.*, 2012, **295**, 45-58.

29   H. Liang, Y. Hong, C. Zhu, S. Li, Y. Chen, Z. Liu, D. Ye, *Catal. Today*, 2013, **201**, 98-102.

30   E. Y. Konysheva, S. M. Francis, *Appl. Surf. Sci.*, 2013, **3**, 14114-14122..

31   E. Armstrong, K. L. Duncan, E. D. Wachsman, *Phys. Chem. Chem. Phys.*, 2013, **15**, 2298-2308.

32   W. Chen, A. Nijmeijer, L. Winnubst, Solid *State Ionics*, 2012, **229**, 54-58.

33   J.N. Kuhn, U.S.Okzan, J. Catal., 2008, **253**, 200-211.

34   L. G. Tejuca, *J. Less-Common Met.*, 1989, **146**, 251-259; X. Niu, H. Li and G. Liu, *J. Mol. Catal. A-Chem.*, 2005, **232**, 89-93.

35   F. Deganello, G. Marcì and G. Deganello, *J. Eur. Ceram. Soc.,* 2009, **29**, 439–450.

36   S. R. Jain, *Explos. Pyrotech.,* 1987, **12**, 188–195; S. R. Jain, K. C. Adiga and V. R. P. Verneker, *Combust. Flame,* 1981, **40**, 71-79.

37   S. Brunauer, P. H. Emmett and E. Teller, *J.Am.Chem.Soc.,* 1938, **60**, 309-319.

38   E. P. Barrett, L. G. Joyner and P. P. Halenda, *J.Am.Chem.Soc.,* 1951, **73**, 373-380.

39   A. C. Larson and R. B. Von Dreele, GSAS General Structure Analysis System, LANSCE, MS-H805; Los Alamos National Laboratory, Los Alamos, NM 87545, USA, 1998.

40   L. B. McCusker, R. B. Von Dreele, D. E. Coxd, D. Louer and P. Scardi, *J. Appl. Crystallogr.,* 1999, **32**, 36–50; B.H. Toby, *Powder Diffraction*, 2006, **21**, 67-70.

41   S. Li, L. Jing, W. Fu, L. Yang, B. Xin and H. Fu, *Mater. Res. Bull.*, 2007, 42, 203-212.

42   G. Magnacca, G. Cerrato, C. Morterra, M. Signoretto, F. Somma and F. Pinna, *Chem. Mater.*, 2003, **15**, 675-687.

43   G. Busca and V. Lorenzelli, *Mater. Chem.*, 1982, **7**, 89; V. Crocellà, G. Cerrato, G. Magnacca, C. Morterra, F. Cavani, S. Cocchi, S. Passeri, D. Scagliarini, C. Flego and C. Perego, *J. Catal.*, 2010, **270**, 125-135.

44   A. A. Davydov, in *Infrared Spectroscopy of Adsorbed Species on the surface of Transition Metal Oxides*, J. Wiley & Sons; ISBN 0-471-91 813-X, Chichester, New York, Brisbane, Toronto, Singapure, 1990.

45   G. Busca, *Catal. Today*, 1998, **41**, 191-206.
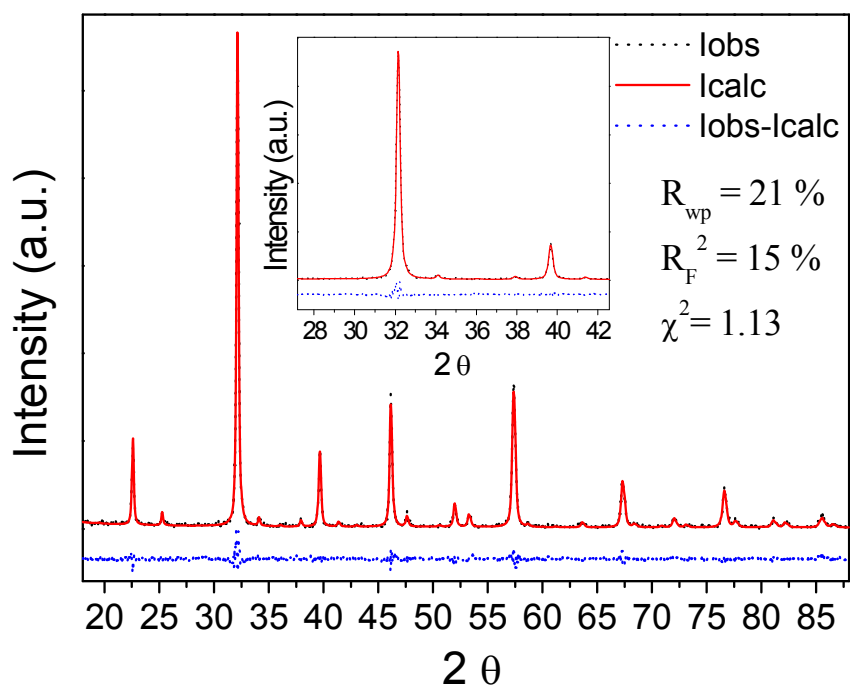
Figure 1: Rietveld Refinement of the XRD data for the LaFeO$_3$ powder calcined at 700°C/5h. The most meaningful discrepancy values (wR$_p$, R$_F^2$ and χ^2) are reported in the figure.
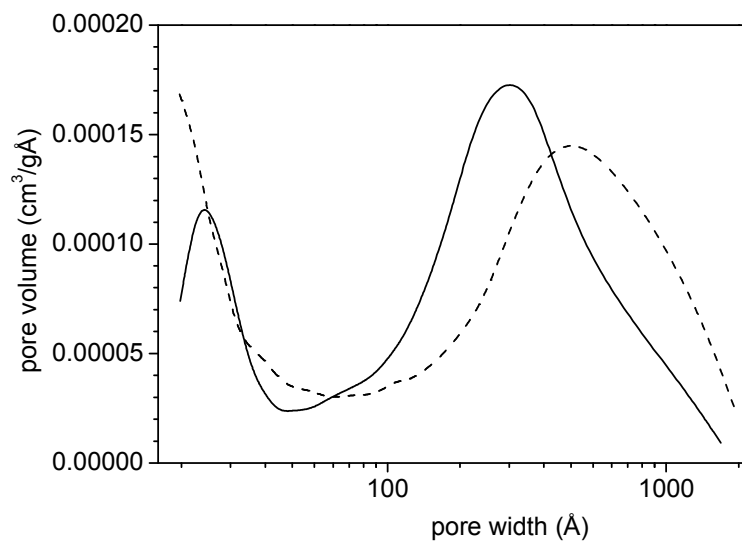
Figure 2 – BJH pore size distributions (from desorption branch) relative to LaFeO$_3$ before (solid line curve) and after (broken line curve) sonication treatment.
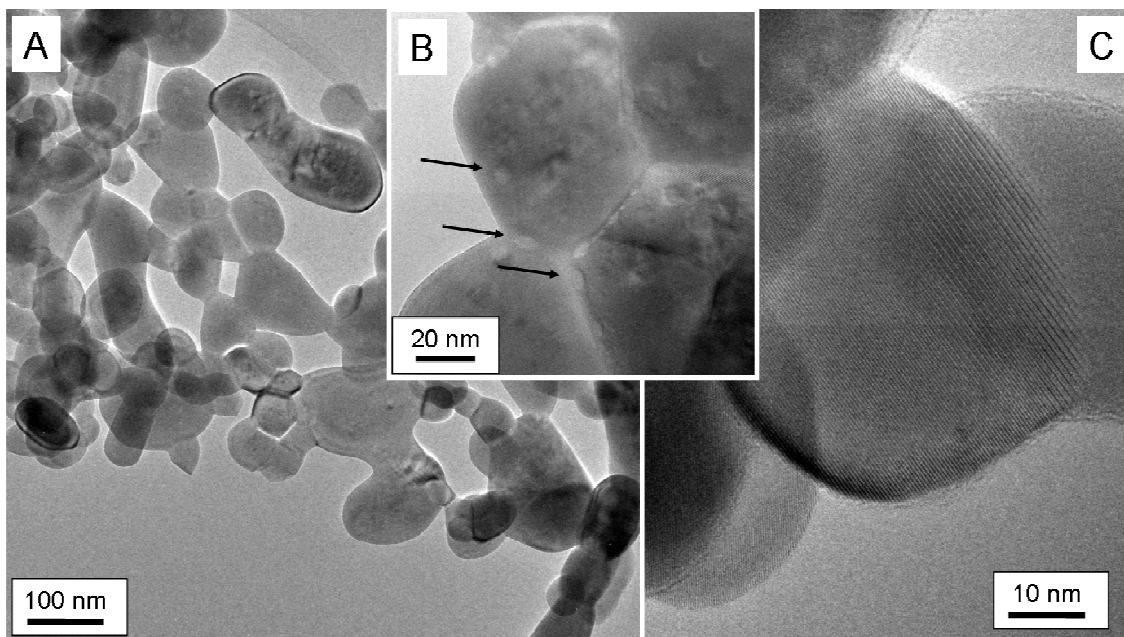
Figure 3 – HRTEM images relative to LaFeO$_3$ sample. The arrows present in section B indicates porosities present at the interface between fused particle and inside the particles.
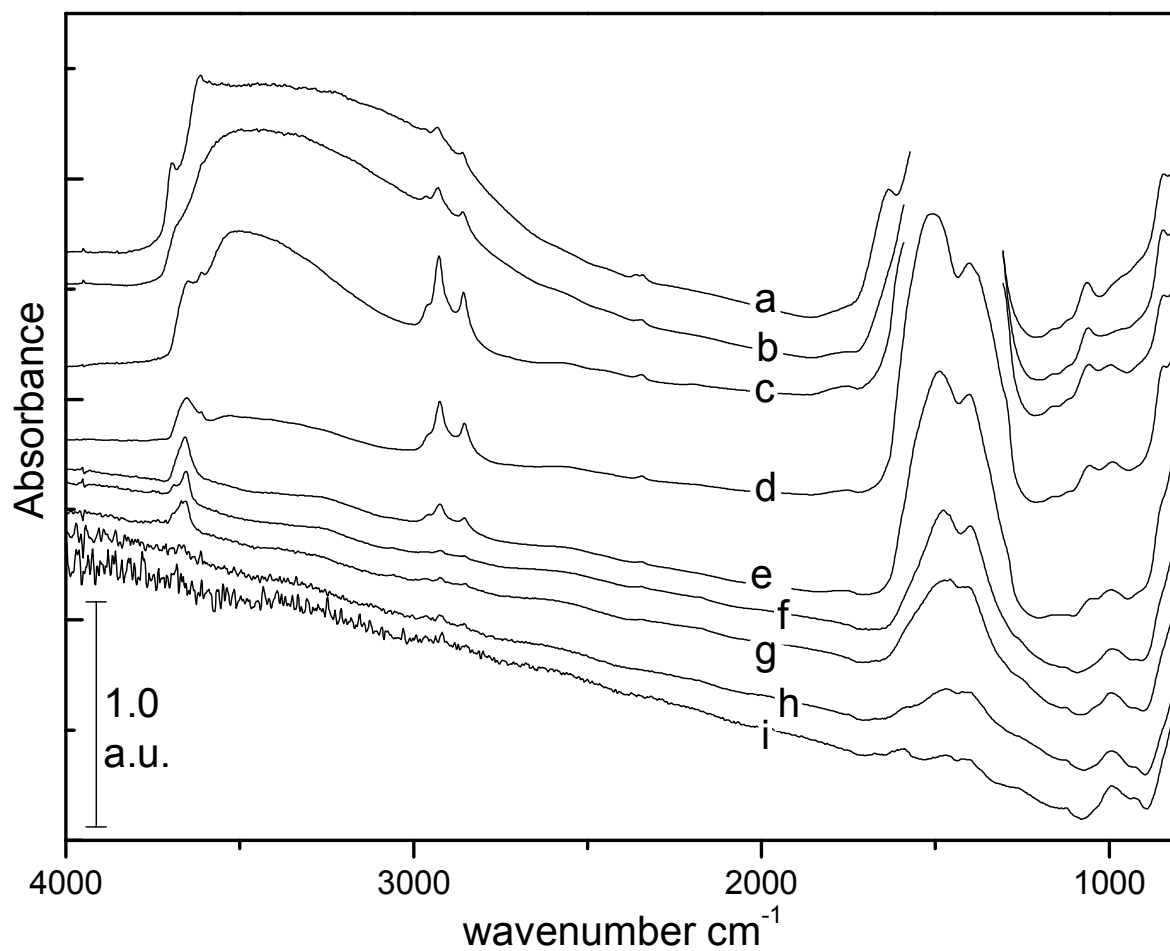
Figure 4 - FTIR absorption spectra of LaFeO$_3$ as it is (curve a), activated for one hour *in vacuo* at RT (curve b), 100°C (curve c), 200°C (curve d), 300°C (curve e), 400°C (curve f), 500°C (curve g), 600°C (curve h) and 700°C (curve i). Curves a, b and c are cut off in the region 1600-1300 cm^{-1} because of the strong intensity shown by the bands.
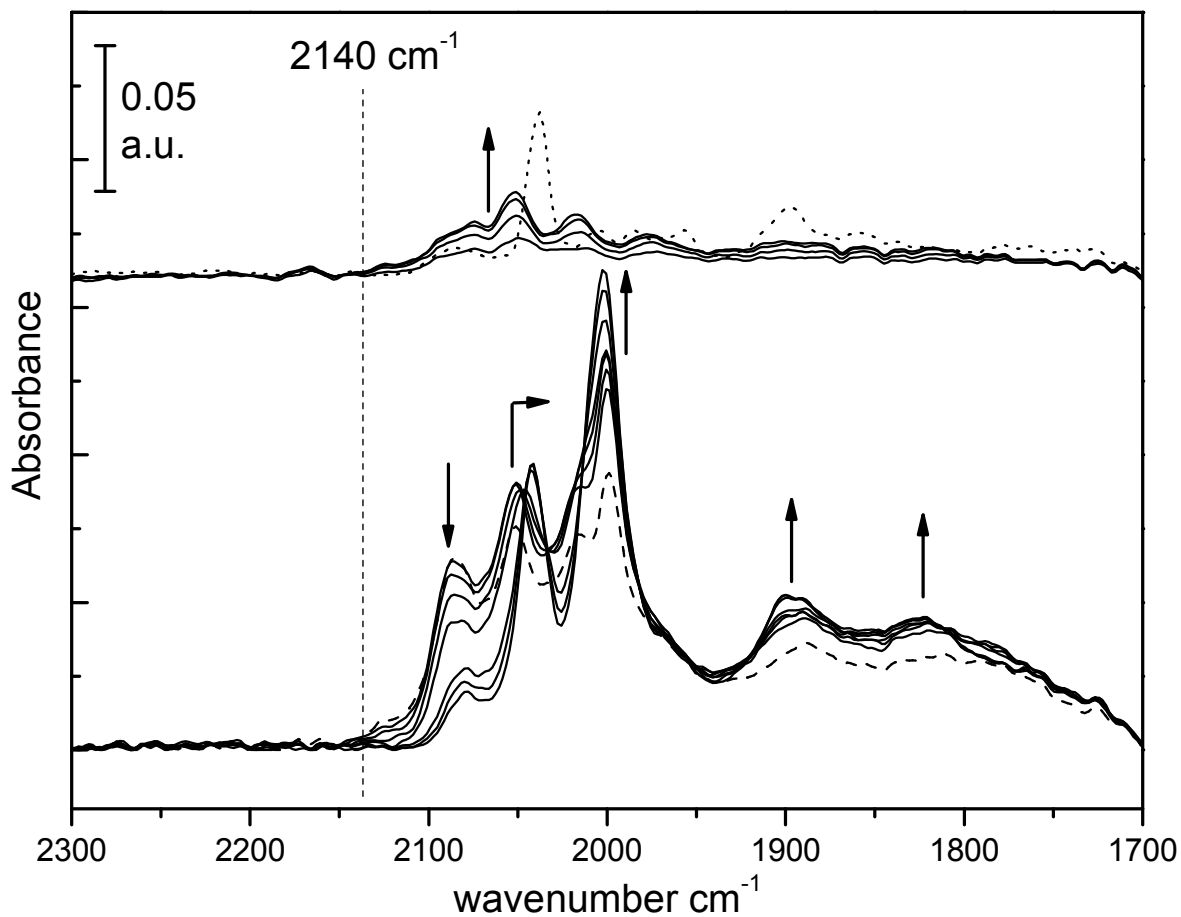
Figure 5 - Differential FTIR spectra in 2300-1700 cm^{-1} range: adsorption of CO on LaFeO$_3$ O400 (upper section) and LaFeO$_3$ R400 (lower section). In the upper section, solid line curves indicate the spectra relative to 100 mbar of CO evolving over time (the upward arrow indicates that absorptions are growing up), dotted line curve is the spectrum after 16 hours of CO contact. In the lower section, broken line curve is relative to the spectrum of 100 mbar of CO and solid line curves indicate the spectra relative to CO pumping off for up to 10 minutes (the upward arrows indicate the components growing up, the downward arrow indicates the component decreasing in intensity, the rightward arrow indicates the red-shift of the component.). The dotted line at 2140 cm^{-1} indicates the spectral limit between CO adsorbed on oxidized (> 2140) and reduced (< 2140) Fe species.
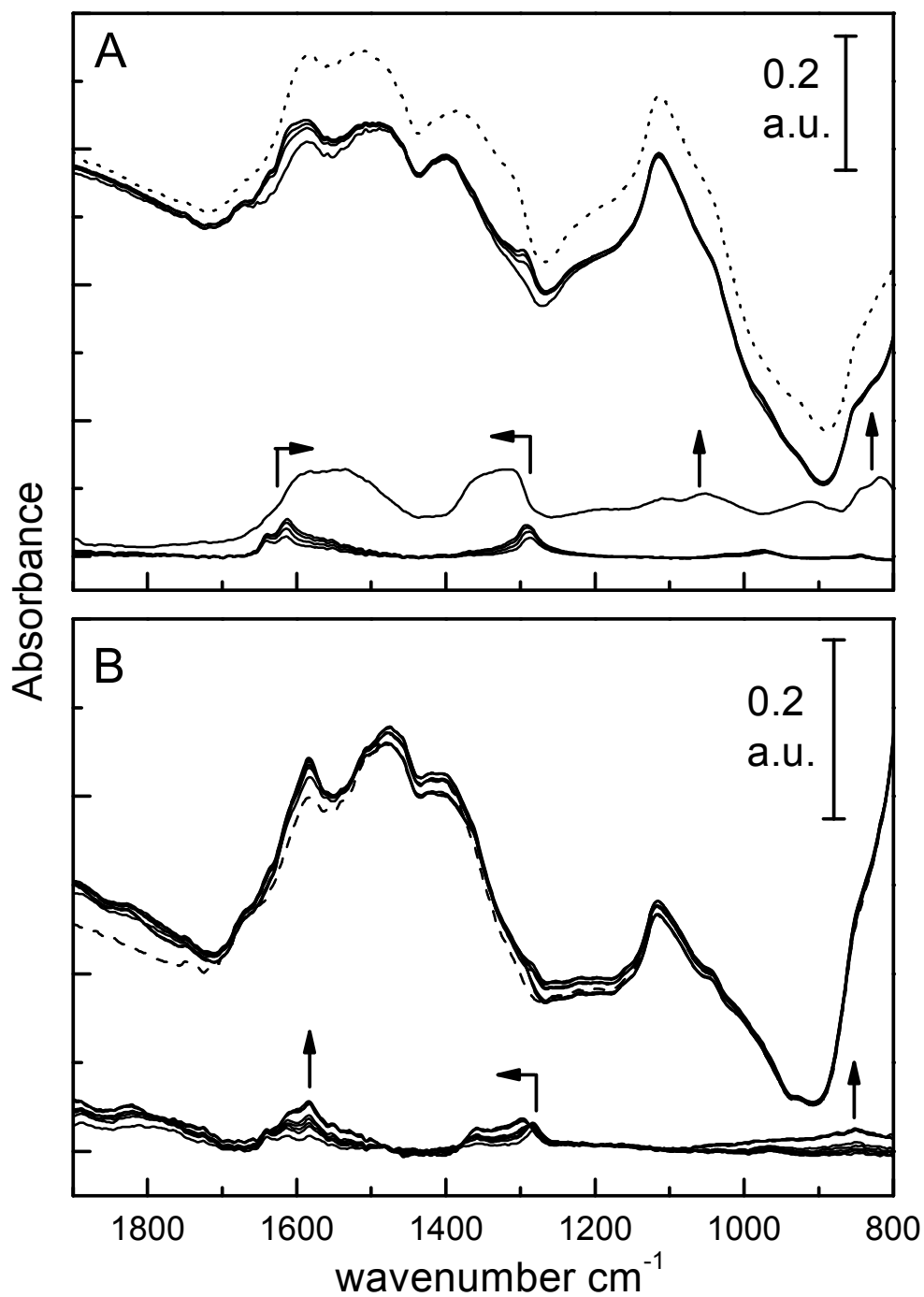
Figure 6A, 6B - Absorption (upper curves) and differential (lower curves) spectra in 1900-800 cm^{-1} range relative to CO interacting with LaFeO$_3$ O400 (section A) and LaFeO$_3$ R400 (section B). In section A solid line curves indicate the spectra relative to 100 mbar of CO evolving over time, dotted line curve is the spectrum relative to 16 hours of CO contact. In section B broken line curve is the spectrum relative to 100 mbar of CO and the solid line curves are the spectra obtained after CO pumping off for up to 10 minutes. The arrows in section A and B indicate the evolution of the components (intensity increase and blue shift) in the differential spectra.
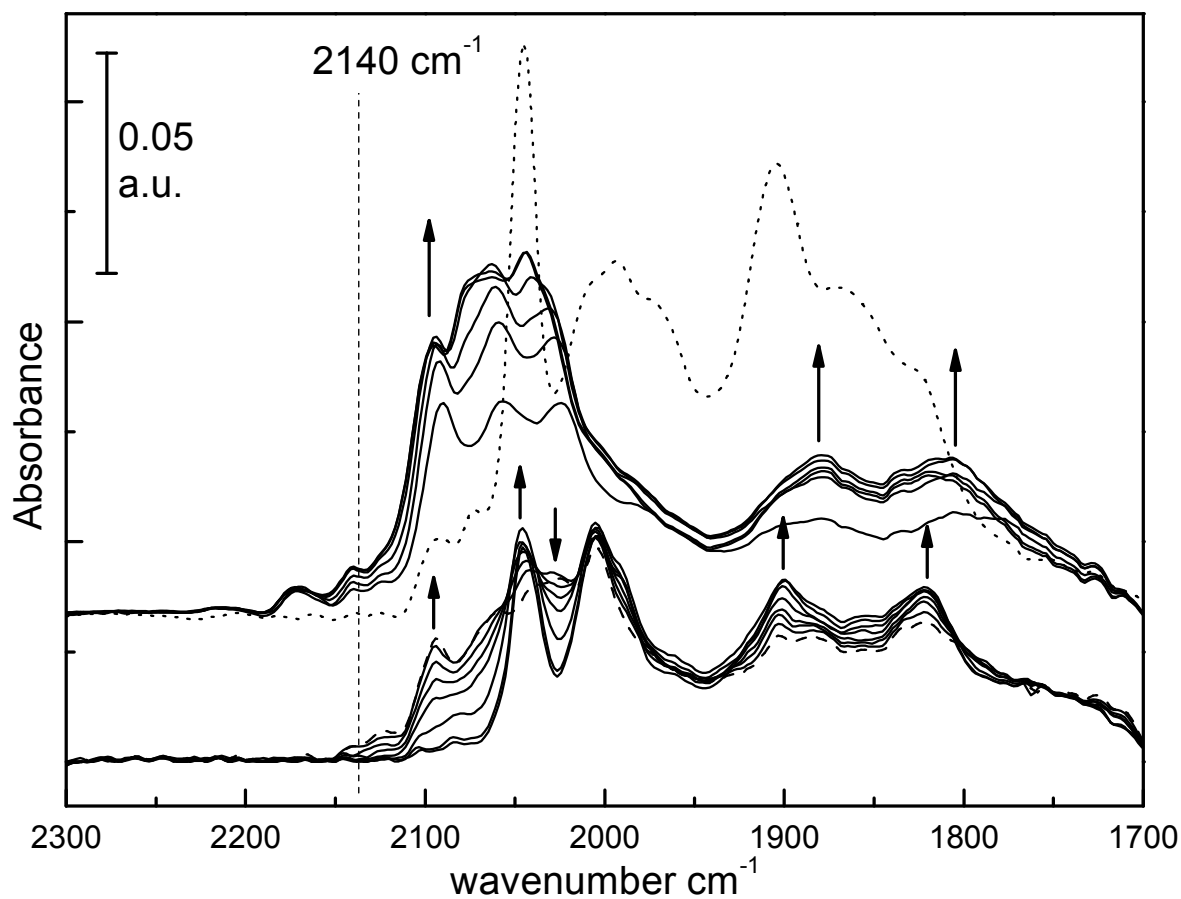
Figure 7 - Differential FTIR spectra in 2300-1700 cm^{-1} range: adsorption of CO on LaFeO$_3$ O700 (upper section) and LaFeO$_3$ R700 (lower section). In the upper section, solid line curves indicate the spectra relative to 100 mbar of CO evolving over time (the upward arrows indicate that absorptions are growing up), dotted line curve is the spectrum after 16 hours of CO contact. In the lower section, broken line curve is relative to the spectrum of 100 mbar of CO and solid line curves indicate the spectra relative to CO pumping off for up to 10 minutes (the upward arrows indicate the components growing up, the downward arrow indicates the component decreasing in intensity). The dotted line at 2140 cm^{-1} indicates the spectral limit between CO adsorbed on oxidized (> 2140) and reduced (< 2140) Fe species.
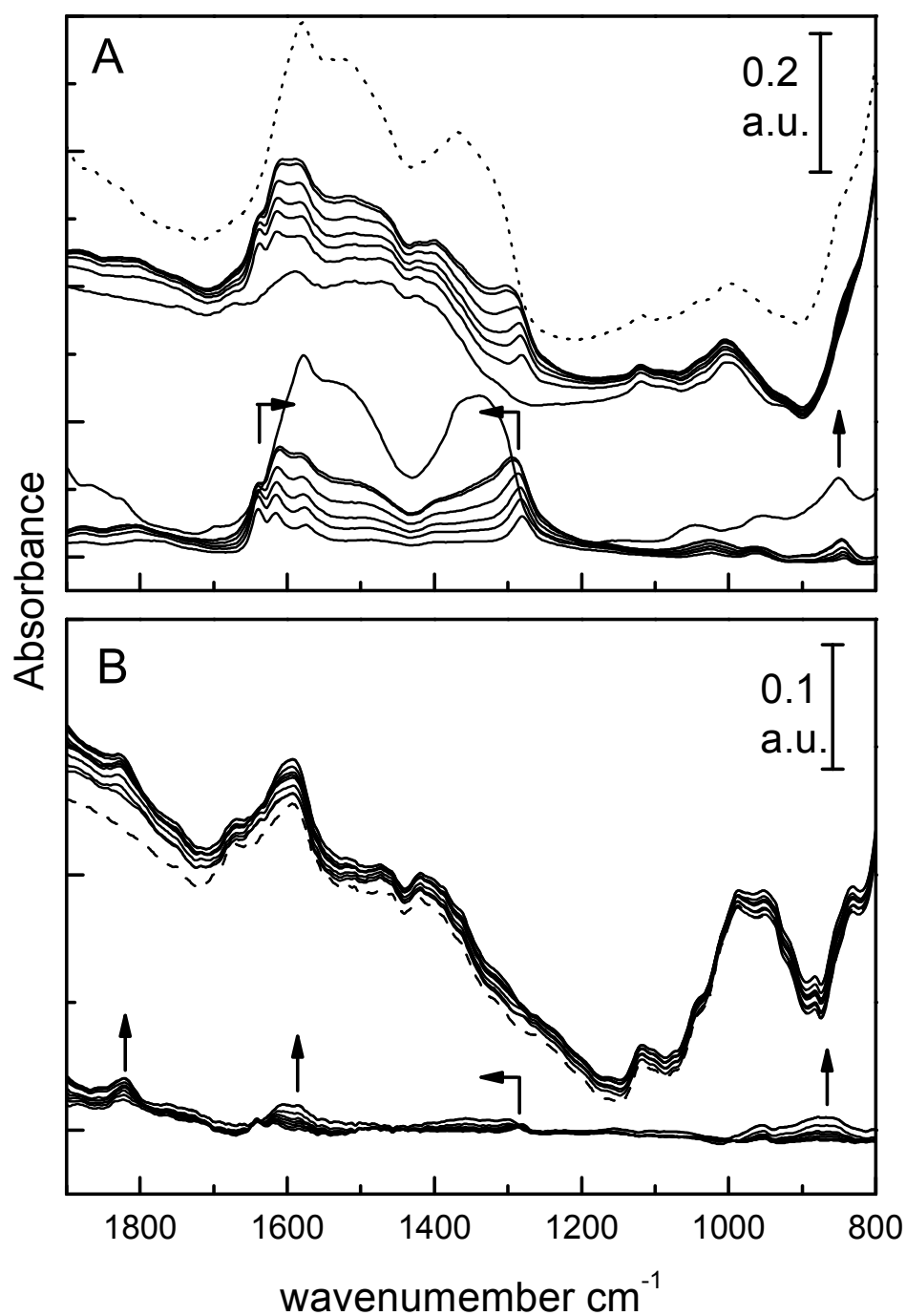
Figure 8A, 8B - Absorption (upper curves) and differential (lower curves) spectra in 1900-800 cm^{-1} range relative to CO interacting with LaFeO$_3$ O700 (section A) and LaFeO$_3$ R700 (section B). In section A solid line curves indicate the spectra relative to 100 mbar of CO evolving over time, dotted line curve is the spectrum relative to 16 hours of CO contact. In section B broken line curve is the spectrum relative to 100 mbar of CO and the solid line curves are the spectra obtained after CO pumping off for up to 10 minutes. The arrows in section A and B indicate the evolution of the components (intensity increase and blue-shift) in the differential spectra.